Size dependent, state-resolved studies of exciton-phonon couplings in strongly confined semiconductor quantum dots

D. M. Sagar, Ryan R. Cooney, Samuel L. Sewall, Eva A. Dias, Mirela M. Barsan, Ian S. Butler, and Patanjali Kambhampati*
Department of Chemistry, McGill University, Montreal, Quebec, Canada H3A 2K6
(Received 9 May 2008; revised manuscript received 3 June 2008; published 27 June 2008)

Coherent optical and acoustic phonons are observed in strongly confined CdSe quantum dots using excitonic state–resolved femtosecond pump/probe experiments. These state-resolved time-domain experiments yield the size dependent exciton-phonon couplings for both modes as well as the excitonic state dependent couplings. The size dependences are weak in this regime, but the state dependence is large for the optical phonons via the Fröhlich interaction. The state dependent coupling to optical phonons suggests that the exciton becomes less polar for higher states. The time-domain data are compared to frequency-domain resonance Raman data. The differences between the various experimental results are discussed in terms of intrinsic versus extrinsic coupling and quantified in terms of the state dependent exciton-phonon couplings.

DOI: 10.1103/PhysRevB.77.235321 PACS number(s): 73.21.La, 78.47.jm, 78.67.Hc, 82.53.Mj

I. INTRODUCTION

Semiconductor quantum dots have been under intense investigation as a key to understanding the physics of exciton confinement, as well as for holding promise in optoelectronic applications.[1–4] One of the longest-standing problems in quantum dot physics is the effect of quantum confinement on the strength of exciton-phonon coupling, a topic that has received considerable experimental[5–21] and theoretical[20,22–28] attention. The strength of exciton-phonon coupling bears relevance to several fundamental issues of nanoscale physics: exciton relaxation dynamics, homogeneous linewidths, and electronic structure.

Optical excitation of quantum dot may result in a hot exciton, in which the electron and/or hole may have excess electronic energy.[2,4,29,30] An early theory suggests that emission by phonons should control the rate of carrier relaxation, thereby yielding a phonon bottleneck for quantized structures.[4,29,31–33] However, later theoretical and experimental works have suggested the presence of additional relaxation channels which would bypass the phonon bottleneck.[4,29,30,34–38] The subtleties in the material parameters and host media of the quantum dot may result in different relaxation pathways and rates, the differences among which can be reconciled by a multichannel picture of exciton relaxation dynamics.[30] Nonetheless, the strength of exciton-phonon coupling is relevant to one of the manifold of pathways by which an exciton in a quantum dot may relax.

Exciton-phonon coupling also bears relevance to the implementation of quantum dots as nonlinear optical materials.[5,6,8–10,25,26] For example, the homogeneous linewidth is a key parameter in such materials. The strength of coupling to phonons in part determines the homogeneous linewidth. Similarly, coupling to phonons may play a role in the resonant Stokes shift between absorption and emission in quantum dots. The earliest theories on the origin of the Stokes shift suggest that it arises due to surface states and/or phonon progressions.[39] The most commonly accepted explanation for the Stokes shift now is that it is due to exciton fine structure.[40,41] However, more recent experiments have suggested that both fine structure and coupling to acoustic phonons play a role in the observed Stokes shift.[19]

A final point of impact is on electronic structure theory. For example, knowledge of the wave functions in a quantum dot enables one to compute the exciton-phonon coupling strength. However, such calculations do not necessarily agree with each other in qualitative structure.[5,6,11,22–28] For example, there is large variance in the computed exciton-phonon coupling strength to optical and acoustic modes. This variance suggests that the appropriate wave functions do not necessarily agree with each other. On a more qualitative level, calculations done under the effective mass $k \cdot p$ approach[3,40,42–44] do not yield the same states and ordering of states as those of an atomistic approach.[38,45–48] The ability to measure the exciton-phonon coupling strength may offer experimental tests of electronic structure theory.

An understanding of the effect of quantum confinement on exciton-phonon couplings will advance the fundamental physics of nanoscale semiconductors as well as provide necessary input to guide materials development for the use of quantum dots as optical materials. Here, we report on size dependent and excitonic state–resolved exciton-phonon coupling in strongly confined colloidal CdSe quantum dots. Femtosecond pump/probe experiments are performed with sufficient time resolution, frequency resolution, and sensitivity to observe coherent optical and acoustic phonons in strongly confined CdSe quantum dots a measure of excitonic state–resolved coupling of optical phonons via the Fröhlich interaction and acoustic phonons via the deformation potential. Size dependent experiments were performed with pumping into the band-edge exciton, which was chosen since it yields the strongest optical and acoustic oscillations. These experiments suggest that the size dependence of the coupling is weak. These time-domain experiments were compared to frequency-domain experiments by analysis of the resonance Raman data. The resonance Raman data (consistent with prior works) yield a much larger optical coupling and no measurable acoustic coupling. The difference between the state-resolved time-domain experiments and the continuous-wave (CW) frequency-domain experiment are reconciled based upon different states being probed in each case.

II. BACKGROUND

Despite several experimental[5–20,49] and theoretical works,[20,22–28] there is presently no consensus as to whether quantum confinement enhances or suppresses the coupling to the relevant optical and acoustic modes. In particular, there are three issues regarding the role of quantum confinement on exciton-phonon coupling in quantum dots: (1) the functional form of the size dependence of the coupling, (2) the absolute value of the size dependence of the coupling, and (3) the excitonic state dependence of the coupling. These issues were addressed by many experimental approaches, but the differences in the results remain unresolved.

The optical modes are coupled via the Fröhlich interaction and the acoustic modes via the deformation and piezoelectric potential in II–VI quantum dots such as CdSe.[5–20,22–27] Theory has predicted either enhancement or suppression of either for both modes, demonstrating the need for experimental determination of the coupling to both modes. Finally, there is a theoretical work which addresses the excitonic state dependence of the coupling strengths,[24] but, to the best of our knowledge, there is no corresponding experimental work. Since quantum dots are characterized by a resolvable eigenstate spectrum,[3,40,42] the state dependent couplings are as relevant to the underlying physics as the more commonly discussed size dependence.

The experimental results have been equally divergent. Many early experiments in quantum dots used CW spectroscopy such as resonance Raman.[11,12,16,23] The Raman experiments in CdSe and other quantum dots suggested extremely large coupling to optical phonons and generally were not able to measure any acoustic modes (except in PbS). Other CW experiments included fluorescence line narrowing[40,50] and single dot photoluminescence (PL) experiments.[21,49,51,52] These experiments also suggested that the optical modes are strongly coupled and the acoustic modes are negligible. One of the more striking observations of the single dot PL experiments was that the coupling strength for a single dot varies by ~20 times *during* the experiment.[21] Finally, very recent single dot PL experiments did observe the confined acoustic modes in strongly confined CdSe quantum dots.[17,18,49]

Prior arguments by Wise,[5] Krauss and Wise,[6] and Efros[53] suggested that the CW experiments do not measure the intrinsic exciton-phonon coupling. They argued that the CW experiments measure the coupling of a quantum dot with trapped charges. These trapped charges build up over the course of the experiment, thereby yielding a more polar quantum dot. This polarized quantum dot would have stronger coupling to optical modes via the polar Fröhlich interaction but would not affect the deformation potential, which is nonelectromagnetic in nature. To circumvent this problem of charging, Wise[5] and Krauss and Wise[6] argued that the intrinsic exciton-phonon coupling should be measured in the femtosecond time domain, prior to the trapping of charges at the surface.

The femtosecond experiments have not fulfilled this promise, being equally divergent in their observations. Early photon echo experiments on CdSe quantum dots observed optical phonons but not acoustic modes.[10] More recent echo peak shift experiments also observed the optical but not the acoustic modes.[8,9] In contrast, echo and pump/probe experiments on PbS quantum dots observed strong coupling to the acoustic modes and extremely weak coupling to the optical modes.[5,6] Finally, pump/probe experiments on CdSe quantum dots observed coherent acoustic phonons but no optical phonons.[13,14] For the purpose of focusing on one material, the canonical strongly confined CdSe quantum dot, the femtosecond experiments have observed either coherent optical or acoustic phonons—but never both. The large variance in the experimental results suggests that there are experimental issues that have to be resolved in order for experiment to provide a clearer test of theory on exciton-phonon interactions in semiconductor quantum dots.

III. EXPERIMENT

Samples of colloidal CdSe quantum dots passivated with organic ligands, hexadecylamine (HDA) and trioctylphosphine oxide (TOPO), were used as received (NN Laboratories). The quantum dots have their band-edge exciton at 619/590/540 nm with corresponding radii of 2.7/1.9/1.6 nm, respectively, estimated from published sizing curves.[54] The linear absorption measurements were performed on a Varian Cary 300 UV-visible spectrometer.

The time-resolved measurements were performed using a regeneratively amplified Ti:sapphire laser system (800 nm, 60–70 fs, 1 kHz, and 2.5 mJ; Coherent) in the transmission pump-probe geometry. The probe pulse was derived from a single filament white light continuum generated in a 2 mm sapphire crystal. The pump pulses were derived from optical parametric amplifiers (OPAs). The pump and probe pulses were compressed using a pair of fused-silica prism compressors. The instrumental response function (IRF) was maintained at ~70 fs full width at half maximum (FWHM) over all wavelength combinations. The pump pulses were generally of ~45 fs FWHM in duration and were transform limited unless otherwise specified. Experiments were performed at two pump wavelengths *simultaneously*, by alternatively chopping each of the pumps such that the pumps appear in the sequence of pump 1, no pump, pump 2.[30,34,35,55] Transients were collected at 333 Hz, corresponding to pump-probe experiments at two different pump wavelengths. Pump normalization was done to nullify the effect of random pump noise. Spot sizes of pump and probe beams were 300 and 50 μm, respectively. Crossing angles of pump and probe beams at the position of sample were 5°.

The CdSe quantum dots were dispersed in toluene and circulated through a 1 mm path length quartz flow cell at 295 K. The mean occupancy $\langle N \rangle$ was obtained by measuring the bleaching saturation curves using published methods.[2,29,56] The pump fluence was set to maintain the same exciton occupancy, $\langle N \rangle = 0.5$, to avoid saturation effects. Under these subsingle exciton conditions, the fractional bleach was ~0.3. The transients probed at the band edge were normalized. The transients with rising edge probe were scaled to the band-edge signal for each pump wavelength. The absorbance of the sample was between 130 and 250 milli–optical density units (mOD). The $\Delta OD/OD$ was about 0.3 at the band-edge exciton. The noise levels were ~0.03 mOD. The step size

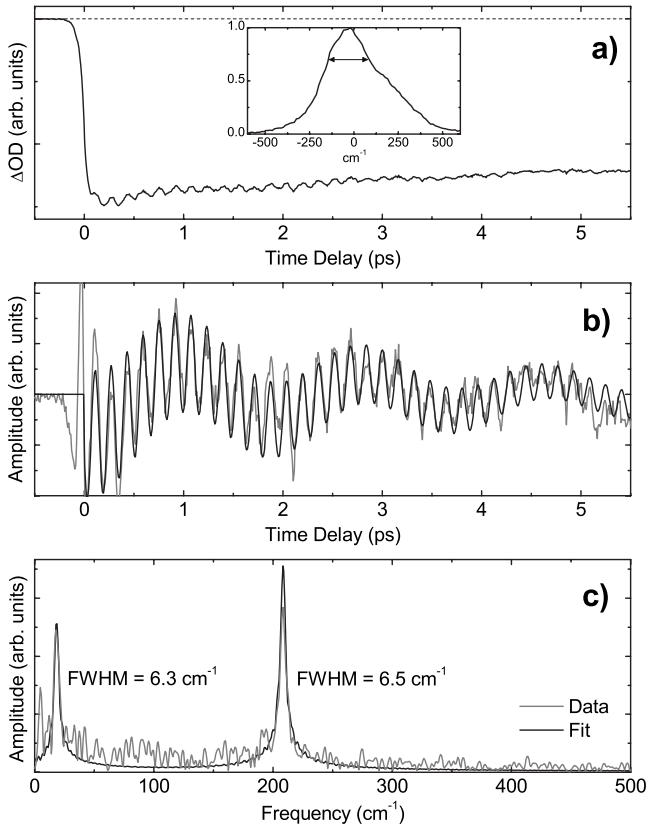

FIG. 1. Simultaneous observation of coherent optical and acoustic phonons in a CdSe quantum dot (R=2.7 nm). (a) A femtosecond pump/probe transient. The inset shows the pump bandwidth relative to the optical-phonon energy. (b) Residual oscillations from the subtraction of the data from the fit. (c) The FFT of the residuals and the fit of the residuals, showing the two coupled modes.

was 10 fs and averaged over 20 sweeps to ensure good signal-to-noise ratio.

Raman measurements were performed using a Renishaw inVia spectrometer equipped with a charge-coupled device detector, a 2400 lines/mm diffraction grating, and a holographic notch filter. The Raman spectra were excited using 514.5 nm argon laser line (Spectra-Physics) with a typical laser power of 1.25 mW. The Raman spectrometer was calibrated prior to each measurement by exciting a silicon sample placed under the microscope and performing an automatic offset correction. The wave-number resolution was 1 cm^{-1}.

IV. RESULTS

A. Simultaneous observation of coherent optical and acoustic phonons in strongly confined CdSe quantum dots

Any effort to quantify exciton-phonon coupling should preferably detect *both* the optical and acoustic modes. Figure 1 shows a femtosecond pump/probe transient of CdSe quantum dots in toluene solution. The transient in Fig. 1(a) shows an IRF limited bleach which recovers on a 10–100 ps time scale. The pump pulse is resonant with the band-edge $1S_e$-$1S_{3/2}$ exciton and has a bandwidth of ~500 cm^{-1} (inset). The probe pulse is tuned on the rising edge of the band-edge exciton, where the derivative of the absorption spectrum is largest.

Provided that the pump pulse has sufficient coherent bandwidth (alternatively, time duration), coherent phonons will be excited. The coherent phonons may then modulate the level structure, thereby yielding a dynamic spectrum. In general, vibrational modulations of pump/probe transients are most prominent where the slope in the absorption spectrum is large;[57–59] hence the probe spectrum was tuned to such a point. Following standard practice in quantum beat analysis of pump/probe experiments, the pump/probe transient was fitted to a model function consisting of a sum of exponentials convolved with the instrument response function.[59,60] In this manner, the nonoscillatory electronic (more precisely, excitonic) contribution to the pump/probe signal is subtracted out. The residual difference between the data and the fits yield the *oscillatory* contributions to the transients [Fig. 1(b)].

The Fourier transform of the residual oscillations yields peaks at 208.4 and 18.4 cm^{-1}, with linewidths of 6.5 and 6.3 cm^{-1}, respectively [Fig. 1(c)]. The peak at 208 cm^{-1} corresponds to the well known, longitudinal-optical (LO) phonon.[8–11,61] The peak at 18 cm^{-1} corresponds to confined longitudinal-acoustic (LA) phonons initially observed in the time-domain experiments[5,6,13,14] and recently observed in the frequency-domain experiments.[17,18]

Quantum size effects are known to yield confined acoustic phonons, with a discrete spectrum.[8,18,26,27] Prior time-domain[5,6,13,14] and frequency-domain[17,18] works have observed individual confined acoustic modes in quantum dots. In particular, the experiments which most cleanly resolve the acoustic modes see only one breathing mode.[6,18] While there may be other acoustic modes in the experimental fast Fourier transform (FFT) spectra (particularly at low frequency), we are able to resolve only one clear acoustic mode, which will be the point of discussion for acoustic phonons. For both LO and LA modes, the data are well fit by exponential decay of the amplitude of the coherence. The time constants are ~5 ps. The FFT of the fit well matches the experimental power spectrum.

Prior time-domain experiments in the canonical strongly confined CdSe quantum dots have observed either coherent optical phonons or coherent acoustic phonons but never *both*.[8–10,13,14] Similar experiments in PbS quantum dots have observed clear acoustic phonons and extremely weak optical phonons.[6] The frequency-domain experiments such as resonance Raman, hole burning, or single dot PL generally observe the LO modes. However, two recent CW experiments were able to observe confined acoustic modes for the first time.[17,18] Here, we see clear evidence that *both* modes are coupled to this band-edge excitonic state, directly in the time domain.

B. Coherent phonons with excitonic state selectivity

All prior works which reported on coherent phonons in strongly confined quantum dots had pump pulses under one of two resonance conditions: pumping directly into the band-

edge exciton[6,8–10] or excitation at 400 nm (3.1 eV).[13,14] The experiments on CdSe quantum dots which observed the LO modes employed the photon echo approach with band-edge excitation. However, no acoustic modes were observed in CdSe quantum dots. In contrast, pump/probe experiments with 400 nm pump yielded observation of only an acoustic mode.

Our recent work on state-resolved exciton dynamics showed that the *initial* excitonic state can have a strong influence on the pump/probe signals.[30,34,35] In particular, the bleaching signals in the transient spectroscopy of quantum dots is well known to arise from state filling.[2,29,30,34,35,56,62] In contrast, the induced absorptions (in the visible regime) in the transient spectra are known to arise from level shiftings related to biexciton formation.[2,29,30,34,35,56,62–64] Upon pumping into specific initial excitonic states, the bleaching and induced absorptions can show marked variations due to the initial excitons populated by the pump pulse.[30,34,35] This *state-resolved* approach has yielded state-to-state exciton relaxation dynamics and has suggested state-resolved studies of biexcitons. These prior state-resolved experiments focus only on the electronic (excitonic) contribution to the pump/probe signal.

These experiments suggest a similar approach in order to probe coherent phonons and exciton-phonon coupling with this *initial state specificity*. Figure 2 shows the state-resolved data on coherent phonons in one size of quantum dot. The pump pulses are tuned to each of the four lowest transitions [Fig. 2(a)]. Only two of the four data sets are shown for the sake of clarity. The description of the excitonic states were taken from prior works.[3,40,42,43] The probe pulse was tuned on the leading edge of the band-edge absorption to maximize the amplitude of the oscillatory portion of the signals.

The pump/probe data for two initial excitonic states are shown in Fig. 2(b). The transient with pumping into the $1S_e$-$1S_{3/2}$ state shows an IRF limited bleach followed by slow recovery.[30,34,35] In contrast, the transient with pumping into the $1P_e$-$1P_{3/2}$ state has an induced absorption which decays on multiple time scales.[30,34,35] The differences between these signals have been previously discussed at length elsewhere[30,34,35] and will not be discussed in detail here. In simple terms, the *nonoscillatory* portions of the signal reflect the *electronic* (excitonic) contributions to the transient spectra via state filling and level shifting.[2,29,30,34,35,56,62–64] We have previously provided a preliminary report on the state dependence of this electronic portion of the pump/probe signal[35] and will discuss it in detail elsewhere.[65] Here, we focus on the *oscillatory* portion of the signal, and its dependence on initial excitonic state.

Subtraction of a model function from these transients reveals the oscillatory residuals [Fig. 2(c)]. In both cases the optical and acoustic modes are visible. While the amplitude of the LA oscillations does not change much, the amplitude of the LO oscillations drops dramatically for higher-energy states. In all cases, the time duration of the pump pulse was nearly the same (40 ± 5 fs), with similar signal-to-noise ratio. The experiments were done with the same number of absorbed photons and were furthermore done *simultaneously* in order to minimize experimental and sample variance. The FFT spectra similarly show the state dependence of the two modes [Fig. 2(d)].

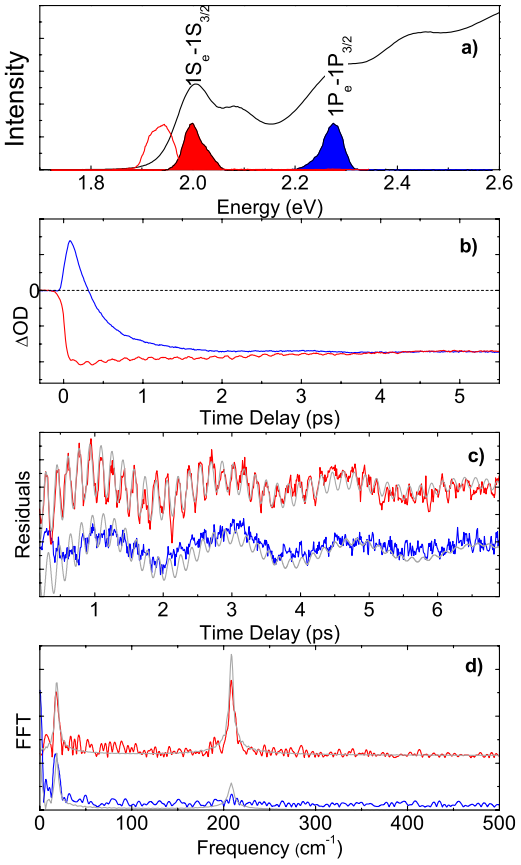

FIG. 2. (Color online) State-resolved coherent optical and acoustic phonons in CdSe quantum dots ($R=2.7$ nm). (a) Linear absorption spectrum, pump spectra (filled), and probe spectrum (line). (b) Femtosecond pump/probe transient corresponding to the pump spectra in (a). (c) Residual oscillations and fits (gray). (d) The FFTs of the residuals and the fits of the residuals (gray).

The strong excitonic *state dependence* of the oscillation amplitude suggests an explanation for the discrepancy between femtosecond experiments. The experiments with band-edge excitation show the LO modes, while the experiments with excitation into higher-lying states at 3.1 eV did not display the LO modes. Our state-resolved results suggest that this discrepancy may be *intrinsic* to the quantum dot itself, rather than to differences in time-domain experiments. An explanation for the absence of LA modes in the photon echo experiments with band-edge excitation is not obvious, however.

C. Size dependence of coupling to the band-edge exciton

This excitonic state–resolved experiment on *one size* of quantum dot immediately suggests a choice in initial excitonic state for *size dependent* investigations. The $1S_e$-$1S_{3/2}$ band-edge exciton has the strongest amplitude for both LO and LA modes. As such, it offers the cleanest window into the size dependence of the coupling to both modes.

Figure 3 shows the size dependence of the coherent phonons under conditions of band-edge pumping. In all cases, the probe spectrum was tuned to the identical point in the linear absorption spectrum—the point of maximum slope

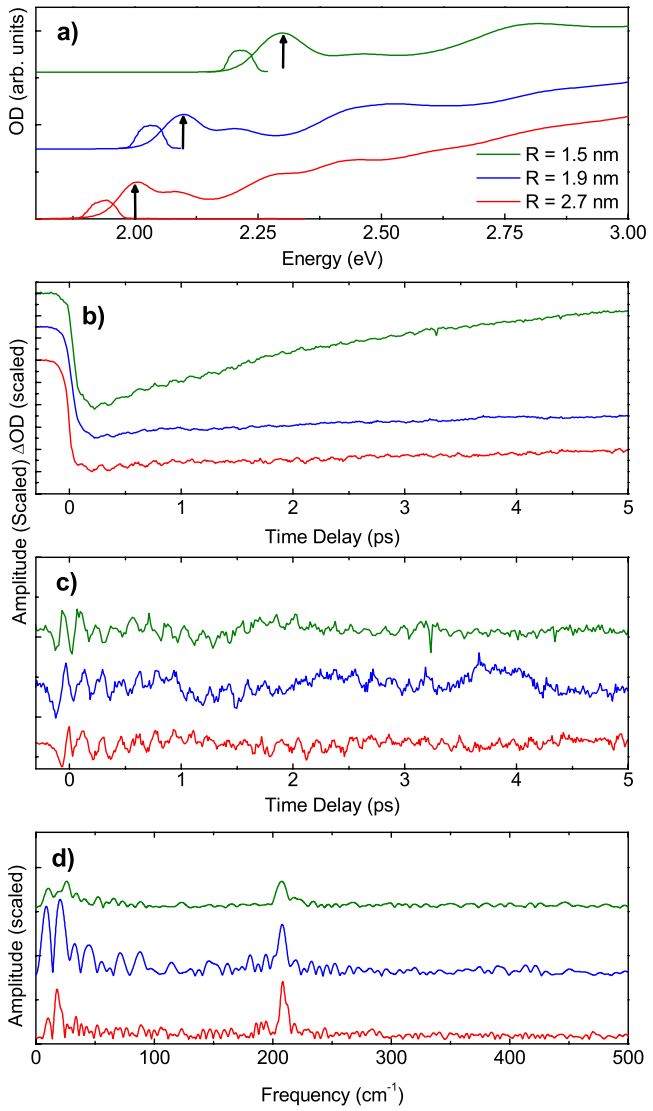

FIG. 3. (Color online) Size dependence of coherent optical and acoustic phonons in CdSe quantum dots with band-edge pumping. (a) Linear absorption spectra and probe spectra. The arrows correspond to the pump position. (b) Femtosecond pump/probe transients corresponding to the three sizes of quantum dots. (c) Residual oscillations. (d) The FFTs of the residuals.

which maximizes the observed oscillation amplitude. Figure 3(b) shows the pump/probe data for three sizes. In all cases, there is an IRF limited bleach which decays on multiple time scales. This behavior has been previously discussed by us and will not be discussed in detail here.[30,34,35] In this spectral region, the excitonic portion of the signal has contributions from both state filling (bleaching) and biexciton induced level shifting (induced absorptions).[2,29,30,34,35,56,62–64] The differences in the envelope of the transients here reflect differences in the extent of the level shiftings due to biexciton interactions. This point was discussed for one size of particle in our prior work[35] and will be discussed in detail elsewhere.[65] Broadly, the envelope of the transients corresponds to the electronic (excitonic) contributions to the signal, whereas the oscillatory portions correspond to the phonon contributions.

Here, we focus only on the oscillations reflecting the phonon dynamics. Figure 3(c) shows the residual oscillations and Fig. 3(d) shows the FFT spectra. The LO-mode amplitude shows some size dependence, whereas the frequency does not. The LA mode shows both size dependent oscillation amplitude and oscillation frequency.

The FFT spectra in the region of the LA modes suggest that there may be more than one mode present. Indeed, calculations have suggested that there should be a spectrum of confined acoustic-phonon modes.[8,26] In contrast, recent experiments on CdSe quantum dots have observed only one or two observable acoustic modes.[13,14,17,18] Here, we see clear evidence of one acoustic mode and some evidence that a lower-frequency mode may also exist. The lower-frequency acoustic mode is very sensitive to fitting and low-frequency noise, so we will not discuss it further. We focus the remaining discussion of the acoustic modes on the strongest mode that we consistently see with the same position and amplitude in all experiments.

D. Coherent phonon frequency modulates the dynamic absorption spectrum

We further investigate the effect of the coherent phonons on the pump/probe signal by varying the probe wavelength. The presence of coherent nuclear motion may modulate the linear absorption spectrum resulting in a *dynamic* absorption spectrum. Most commonly, one considers that the vibrational wave packet (coherent phonon) modulates the *level structure* via exciton-phonon coupling.[57,58,66,67] In this manner, the oscillating level structure would appear as a *frequency modulated* (FM) dynamic spectrum [Fig. 4(a)]. However, recent experiments have suggested that nuclear wave packets can also modulate the *transition moment* via non-Condon effects.[59,68,69] In this manner, the oscillating transition moment would appear as an *amplitude modulation* (AM) of the dynamic spectrum [Fig. 4(b)]. In *both* cases, a pump/probe transient recorded at a single probe wavelength would yield oscillations. However, transients recorded at *two* probe wavelengths would show differences based upon the mechanism behind the modulations.

In the case of amplitude modulation, all probe wavelengths would show oscillations *in phase*. In contrast, frequency modulation would show *phase shifts* based upon the probed regions. For example, oscillations probed at the red and blue edges of a band would be out of phase by π. The phase shifts in the oscillations based upon probe wavelengths can yield assignment of frequency versus amplitude modulation.

Figure 4(c) shows the linear absorption spectrum and the two probe spectra used to further analyze the oscillations. The probe spectra are tuned to the rising edge and the peak of the band-edge exciton. The trailing edge of this band is not useful since it immediately rises into the next band. Figure 4(d) shows that the oscillations corresponding to these probe spectra are out of phase by precisely the amount $(\pi/2)$ expected for *pure frequency modulation*, within the experimental uncertainty. The phase uncertainty is given by the timing uncertainty of ± 10 fs, corresponding to $\pi/8$ in the

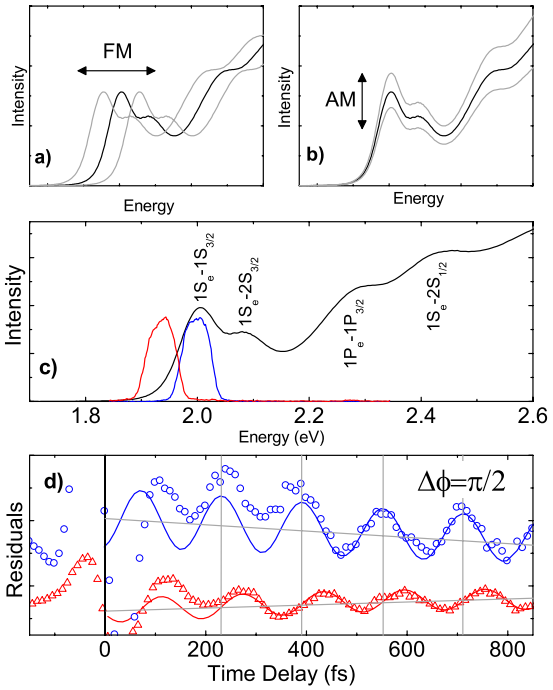

FIG. 4. (Color online) Probe wavelength dependence of oscillation phase. The oscillations arise primarily from frequency modulation. Illustrations of frequency modulated (a) and amplitude modulated (b) spectra. (c) Linear absorption spectrum and the probe spectra. (d) Residual oscillations showing a $\pi/2$ phase shift for the optical phonon. The symbols are the data and the lines are the fits. The gray lines are for guiding the eye. The apparent slope is due to the acoustic phonon.

phase angle. The probe wavelength dependence of the oscillation phase shows that the coherent phonons modulate the level structure, resulting primarily in *frequency modulation* of the dynamic spectrum.

E. Resonance Raman spectra of CdSe quantum dots

The resonance Raman spectroscopy of quantum dots has been discussed in detail elsewhere[11,12,23] and will be discussed only briefly here. Resonance Raman spectroscopy can yield the exciton-phonon coupling strengths based upon a variety of observables such as the Raman excitation profiles and relative intensities of the various modes and their overtones. Figure 5 shows resonance Raman data of CdSe quantum dots ($R=2.7$ nm) in toluene with various passivations of organic ligands or a wide gap semiconductor shell. The data here are qualitatively consistent with prior works so an exhaustive study was not deemed necessary. The objective is to have data on the same quantum dots as used in the femtosecond experiments in order to quantify the *discrepancies* between the methods.

In all cases, one observes both the fundamental and the overtone of the LO mode. The present experiment cannot detect the low-frequency LA mode. We see no evidence of combination modes of LO+LA. The relative integrated areas of the overtone/fundamental are 0.3–0.4, similar to those in prior works. The main point is that this ratio is sensitive to

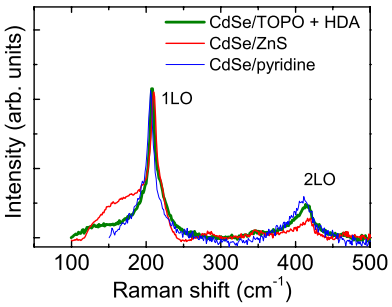

FIG. 5. (Color online) The resonance Raman spectra of CdSe quantum dots ($R=2.7$ nm) with three different surface passivations. The quantum dots are normally passivated with ligands such as TOPO and HDA. Pyridine is a known hole acceptor which will polarize the charge distribution. The ZnS shell best passivates the quantum dot, thereby minimizing surface trapping away from the quantized core states.

surface passivation. A ZnS shell is well known to better passivate the core states, thereby attenuating surface/interface trapping.[29,56,70] In contrast, pyridine is a known hole trap which should amplify (or at least accelerate) the surface trapping process.[29,56,70] The overtone/fundamental intensity ratio, which reflects the strength of the coupling, increases as the surface becomes passivated to induce surface trapping.

V. DISCUSSION

A. Theory of exciton-phonon coupling in quantum dots

1. Optical phonons

The physics of exciton-phonon coupling in semiconductor nanocrystals has been addressed theoretically by various researchers.[22–28] We briefly review the salient features of the coupling mechanism in order to make correspondence to the experimental data. Schmitt-Rink *et al.*[25] estimated theoretically the exciton-phonon coupling in an extremely confined quantum dot where the kinetic energy of the carriers dominate over the phonon energy. In this case the exciton-phonon coupling constant, which is proportional to the difference in the Fourier-transformed wave functions between an electron and a hole, vanishes, thus giving zero or little contribution to the exciton-phonon coupling. Schmitt-Rink *et al.*[25] assumed that the hole is localized at the center of a sphere, giving a delta-function-like density of states, and concluded that the exciton-phonon coupling is size independent. Their study did not take into account the crucial aspect of valence-band mixing and the degeneracy of the valence band. Such a treatment is essential in determining phonon contributions to exciton relaxation since the exciton-phonon coupling depends sensitively on the choice of wave functions. While the basic physics of the coupling is well understood, the practical implementation of these calculations is not straightforward. For example, the calculated couplings can vary by *orders of magnitude* based upon material parameters. More specifically, a precise determination of wave functions of both electron and hole is necessary to obtain accurate values of the coupling strengths.

A more realistic treatment taking into account valence-band mixing was performed by Nomura and Kobayashi.[24] They pointed out that the main ingredients for treating the wave functions are, to begin with, confinement energy and the phonon energy. When the former is larger than the latter, the excitonic relaxation through phonons is small and the system can be treated in first order with the independent-phonon model. The opposite limit leads to bulk semiconductor properties. The theory by Nomura and Kobayashi[24] treats the physics of exciton-phonon coupling by taking into account the valence-band mixing and nonparabolicity in the strong confinement limit[3,40,42,43] and leads to a more realistic value of exciton-phonon coupling in semiconductor quantum dots.

The work of Nomura and Kobayashi[24] accounts for the moderate coupling strengths ($S \sim 0.02-0.04$) obtained for LO phonons in the present study. The confined LO phonons are considered within the continuum model. This model gives good approximation for quantum dots with radius sufficiently larger than the lattice constant. The displacement of ions ($\mathbf{u}$) can be written as,

$$(\nabla^2 + k^2)u = 0, \tag{1}$$

where k is the mode frequency of phonons and u is the displacement. Depending upon the nature of the displacement u, there can be two solutions pertaining to freestanding wave and a rigid wave at the boundary. The solution of Eq. (1) is given as

$$u_r = C_{nl} j_l'(q_{ln} r) Y_{lm}(\theta, \phi), \tag{2}$$

$$u_\theta = C_{nl} \frac{j_l'(q_{ln} r)}{q_{ln} r} \frac{\partial}{\partial \theta}(Y_{lm}(\theta, \phi)), \tag{3}$$

$$u_\phi = C_{nl} \frac{j_l'(q_{ln} r)}{q_{ln} r} \frac{im}{\sin\theta}(Y_{lm}(\theta, \phi)), \tag{4}$$

where C_{nl} is the amplitude of the mode n, l and j's are the spherical Bessel functions. The solutions are given in the cylindrical coordinates. The Huang-Rhys parameter S_λ is given by

$$S_\lambda = \frac{f_0^2}{(2\pi)^3} \int d^3k \frac{1}{k^2} \frac{|\nu_{\lambda\lambda}(k)|^2}{(\hbar\omega_{\mathrm{LO}})^2}, \tag{5}$$

where $\hbar\omega_{\mathrm{LO}}$ is the energy of the LO phonons, k is the wave vector, f_0 is the Fröhlich interaction coupling constant, and $n_{\lambda\lambda}(k)$ is the phonon wave function. It is assumed that the polarization of ions is proportional to their displacement. This leads to the phonon potential of the form

$$\Phi = 4\pi U \frac{C_{nl}}{q_{nl}} j_l(q_{ln} r) Y_{lm}(\theta, \phi), \tag{6}$$

where U is determined by the size dependent dielectric constants. The exciton-phonon interaction Hamiltonian is given by

$$\hat{H}_{\text{ex-ph}} = e \int d^3r_1 d^3r_2 \psi_\lambda^* \psi_\mu [\Phi(r_2 - \Phi r_1)], \tag{7}$$

$$\hat{H}_{\text{ex-ph}} = \sum \frac{f_0}{q_{ln} R^{3/2}} v_{\lambda\mu}(q_{ln})(a_{q_{ln}} + a_{q_{ln}}^\dagger). \tag{8}$$

Here R is the radius of the nanocrystal. It should be noted that a finite exciton-phonon coupling is obtained only by including the effect of valence-band mixing. In the absence of valence-band mixing, the electron and hole wave functions are identical in the strong confinement limit and hence vanish, giving no contribution to the coupling.

By using the appropriate wave functions and substituting into Eq. (3), the exciton-phonon coupling is given by

$$S_\lambda = \frac{f_0^2}{R^3} \sum_{q_{ln}} \frac{1}{q_{ln}^2} \frac{|\nu_{\lambda\lambda}(q_{ln})|^2}{(\hbar\omega_{\mathrm{LO}})^2}. \tag{9}$$

One may notice that the Huang-Rhys parameter is proportional to R^{-3}. The LO phonon frequency is weakly size dependent. It was shown by Nomura and Kobayashi[24] that for $R < 7$ nm, the Huang-Rhys parameter increases with exciton confinement due to the coupling of the excitonic state with higher-frequency phonons.

It is convenient to recognize two regions based on the interplay between the exciton confinement energy and Coulomb interaction energy. For $R < 7$ nm, S increases with decreasing nanocrystal radius or, in other words, confinement energy in CdSe. For dots of larger radius, the coupling increases upon increasing the radius due to an increase in the Coulomb energy. The cross-over region from strong confinement to Coulomb regime is determined by the choice of the Luttinger parameters, which are in turn determined by the difference in the electron and hole masses. These theoretical predictions are verified in our experiments.

The Huang-Rhys parameter calculated by Nomura and Kobayashi[24] is on the order of 0.03–0.08 depending on the choice of the Luttinger parameters.[24] A recent implementation of their approach yielded $S = 0.002-0.03$ for self-assembled pyramidal quantum dots.[20] It should be noted that the Luttinger parameters are rather sensitive to the splitting of the hole sub-bands and hence to the particular geometry of the valence-band curvature. The valence-band splitting and its geometry depend on the crystal structure. As can be seen in the study of Nomura and Kobayashi,[24] the exciton-phonon coupling strength depends considerably on the choice of Luttinger parameters and hence on the finer details of the valence-band curvature, which determines the hole masses and hence the kinetic energy of the carriers. As mentioned earlier, the kinetic energy of the carriers is a crucial parameter together with the phonon energy.

2. Acoustic phonons

The role of acoustic phonons in excitonic dephasing has been experimentally observed by various researchers. Specifically, the linear temperature dependence of excitonic dephasing rate suggests the importance of exciton–acoustic phonon interactions. The physics of acoustic phonons in nanocrystals was addressed by Takagahara.[26,27] In the limit that the nanocrystal radius is not too small, the acoustic properties can be described in terms of the elastic vibrations of a homogeneous sphere.[5,6,8,18,26,27] While we do not discuss the

theory extensively, we discuss the salient features of the theory and its relevance to our experimental results.

The vibrations of an elastically isotropic sphere are described by

$$\rho\frac{\partial^2}{\partial t^2}u = (\lambda + u)\text{grad div}\ \ u + \mu\nabla^2 u, \tag{10}$$

where u is the lattice displacement vector, ρ is the mass density, and λ and μ are the Lamé constants. As proposed by Lamb for the first time, the equation has two eigenmodes, namely, torsional modes and spheroidal modes. For spheroidal modes, the displacement vector is given by

$$u(r) = p_{lm}L_{lm}(hr) + q_{lm}N_{lm}(kr). \tag{11}$$

Here, p and q are some coefficients and the eigenfrequency is related to h and k by $\rho\omega^2=(\lambda+2\mu)h^2=\mu k^2$. L's and N's are the spherical harmonics which determine the nature of the wave functions.

It should be noted that these spherical harmonics do not take into account the precise nature of the excitonic states. In other words, in order to determine precisely the exciton-acoustic phonon coupling strengths, one needs to have precise knowledge of excitonic wave functions. Thus, this simple theory may not account for the experimentally observed coupling strengths since this involves the finer details such as valence-band structure, nonparabolicity, and shape asymmetry of the quantum dots. Nevertheless, the elastic continuum model accounts for the observed size dependent frequency of acoustic modes. For deformation potential, the eigenfrequency of the modes scales as $1/R$, verified in our experiments as well. As argued by Takagahara,[26,27] for strongly confined quantum dots ($R<5$ nm), the deformation potential coupling dominates over the piezoelectric coupling.

As shown by Salvador *et al.*,[8] the calculated reorganizational energy is on the order of μeV, which is about 3 orders of magnitude smaller than the value obtained from our experiments (see Secs. V B and V C). The discrepancy can be readily explained by the usage of Bloch functions for calculating the electron-hole wave functions. For example, the choice of more tightly bound wave functions enhances the coupling by a few orders of magnitude.[8] This large variance in the calculated couplings demonstrates the need to incorporate the effects on certain sensitive physical variables such as valence-band degeneracy, excitonic fine structure, and phonon confinement energy. Based on our experimental results and the previous theoretical work by Salvador *et al.*,[8] we suggest the need for a theory that takes into account exciton wave functions (fine structure) and acoustic-phonon coupling. Similar points were made in light of recent temperature dependent Stokes shift in these materials.[19]

B. State-resolved exciton-phonon couplings

The question of the *excitonic state dependence* of exciton-phonon coupling is a point which has received little attention. Early work by Nomura and Kobayashi[24] may be the only theoretical work that considered this point. To the best of our knowledge, no experiment aimed to measure the excitonic state dependence of the coupling strength. The simplest reason for measuring state-resolved exciton-phonon coupling is that a discrete eigenstate spectrum is one of the key features of semiconductor quantum dots.[1–4,30,34,35,40,42,43] The vast majority of experiments which address quantum dot physics generally do so as a function of *particle size*, since these are confined semiconductors. Since the confinement itself induced quantized states, the *eigenstate dependence* of the relevant physical parameters also seems to merit investigation.

One reason for examining *state-resolved* exciton-phonon couplings is that a rigorous investigation of intraband relaxation dynamics should require an understanding of the *eigenstate-specific* coupling strengths. For example, exciton relaxation dynamics broadly follow state-to-state quantum dynamics with a transition rate which may have contributions from phonon based pathways.[30,34,35] As such, the coupling strength for each state is relevant. Similarly, recent work by Liptay *et al.*[19] suggested the importance of *state-specific* couplings to acoustic phonons in understanding the temperature dependence of the PL spectra. Finally, one might expect that the discrepancies between different experiments may be resolved based upon differences in the initial (or final) excitonic states.

The data in Figs. 1 and 2 show that the oscillation amplitudes and therefore coupling strengths are sensitive to the initial excitonic state into which the pump pulse is resonant. The oscillation amplitudes can be related to the exciton-phonon coupling strengths by virtue of the assignment of frequency modulation of the dynamic absorption spectrum. Since the dynamic spectrum is dominantly frequency modulated (within the phase uncertainty of $\pm\pi/8$), the oscillation amplitude *directly* reflects the magnitude of the level shiftings [Fig. 4(a)]. The amplitude of the oscillations reflects the reorganization energy or frequency modulation amplitude via

$$A_{\text{osc}} = \left(\frac{d\text{OD}}{d\omega}\right)\Delta\omega. \tag{12}$$

OD is the optical density of the linear absorption spectrum measured at the sample position, A_{osc} is the amplitude of the oscillations in the same units, and $\Delta\omega$ is the energy shift, or alternatively, the reorganization energy (coupling strength in energy units). The point is that these experiments allow *direct* estimation of the energy shifts.

The exciton-phonon coupling strengths are noted by the set of parameters $[\Delta, S, \lambda]$, where Δ is the dimensionless displacement of the normal coordinate, S is the dimensionless Huang-Rhys parameter ($\Delta^2/2$), and λ is the reorganization energy ($\hbar\omega_{\text{phonon}}S$). The phonon modes are treated as displaced harmonic oscillators with a displacement Δ and a resultant coupling strength in energy units, λ. The excitonic state–resolved ($1S_e$-$1S_{3/2}$) coupling strengths for the optical mode are [0.23, 0.026, 0.68 meV]. The couplings for the acoustic mode are [0.81, 0.33, 0.73 meV]. The state-resolved exciton-phonon couplings are shown in Fig. 6 for a CdSe quantum dot of 2.7 nm radius (2.00 eV band-edge exciton). The uncertainties in the coupling strengths arise from uncertainties in the AM/FM assignment ($\pm 25\%$ of the amplitude). For the sake of simplicity, we assume that oscillation amplitude has contributions both from excited-state and ground-

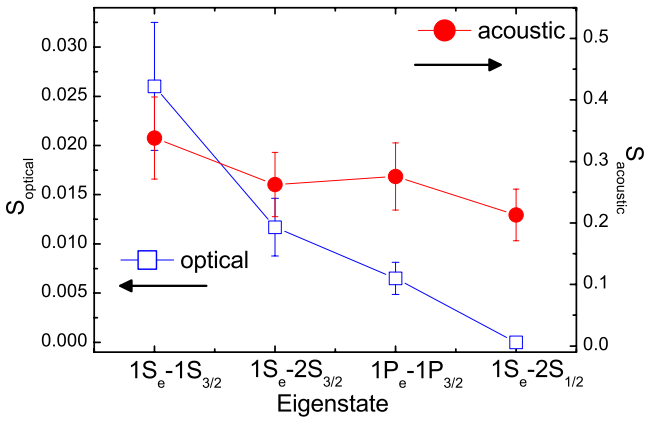

FIG. 6. (Color online) The excitonic state–resolved coupling strengths (S) to optical and acoustic phonons for a CdSe quantum dot (R=2.7 nm). The eigenstates and coupling strength (S) are discussed in the text.

state wave packets. In principle, one or the other could dominate,[57,58] a point which will be addressed elsewhere.[71] This assumption will not change the general form of the results but could change the absolute values by a factor of 2.

These state-resolved measurements show that the oscillation amplitudes and coupling strengths are nearly equal for the optical and acoustic modes, under the condition of band-edge excitation (Figs. 1–5). The oscillation amplitude and coupling strength for the LO phonons drop steeply as a function of the eigenstate, whereas the LA amplitude is weakly dependent on state. This state dependence to the coupling strength may reconcile the differences between prior experiments. For example, the echo experiments on CdSe quantum dots were all done under conditions of band-edge excitation.[8–10] The echo experiments yielded qualitatively similar results for LO coupling; however, the LA modes were not observed. The reason for the absence of LA modes in the echo experiments will not be discussed here. The pump/probe experiments which observed the LA modes were all done under excitation at 3.1 eV,[13,14] well into the higher-lying excitons. Based upon the lowest four eigenstates, excitation at 400 nm may not yield LO modes simply because the couplings are small. These coupling strengths for the LO modes are much smaller than reported in the literature using CW spectroscopies. This result is entirely consistent with the prior arguments by Wise,[5] Krauss and Wise,[6] and Efros[53] and will be further discussed below.

The experimentally determined state dependent couplings suggest that the Fröhlich coupling to optical modes drops dramatically for higher excitonic states, whereas the deformation potential coupling to acoustic modes moderately decreases. The Fröhlich coupling involves the interaction of the polar optical phonons with the polarization of the exciton. As such, the eigenstate dependence reflects the degree of polarization of the manifold of states. The net polarization of the exciton reflects a confluence of effects such as confinement energy, nonspherical shape, differing effective masses, valence-band couplings, and nonparabolicity.

The excitonic state dependence of S_{LO} suggests that the higher-lying states are less polar by virtue of a smaller polarization based Fröhlich coupling. One might attempt a simple rationalization of this result in terms of the wave functions under the envelope approximation. For example, the higher states should have more nodes, are more diffuse, tunnel further into the surrounding matrix, etc. However, a simple rationalization may not be meaningful, considering the theoretical works greatly diverge even on the net polarization (coupling) of the *band-edge exciton*. We note that the early work by Nomura and Kobayashi[24] suggested similar state dependent couplings. However, the excitonic states themselves do not necessarily agree with each other.[3,38,43–48] The divergence between experimental and theoretical works demonstrates the need for measurements of the relative as well as state dependent couplings for both optical and acoustic modes.

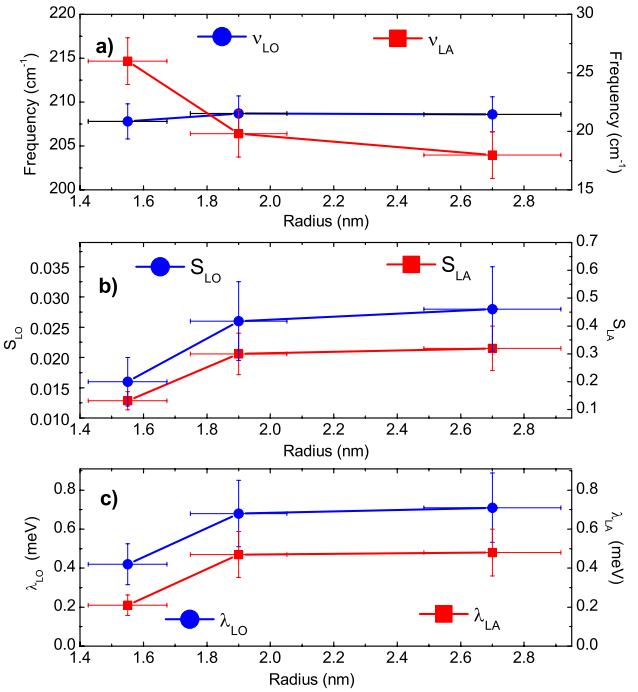

FIG. 7. (Color online) The size dependence of the optical- and acoustic-phonon parameters under conditions of band-edge pumping. (a) The size dependent frequencies. (b) The size dependent Huang-Rhys parameter S. (c) The size dependent reorganization energy λ.

C. Size dependent exciton-phonon couplings

The size dependence of the exciton-phonon coupling is considered for excitation into the band-edge exciton. Here the oscillation amplitudes are strongest and many femtosecond and CW experiments are performed under resonance with the band-edge exciton. Figure 7 quantifies the size dependence of the LO and LA parameters for these experiments.

The frequency of the LO phonon is weakly, if at all, size dependent [Fig. 7(a)]. In contrast, the LA mode frequency is clearly size dependent. This behavior has been previously considered[5,6,13,14,18,72] and will not be discussed in detail here. The coupling strengths are weakly size dependent for

both modes in this size regime [Fig. 7(b)]. While the LA mode has a larger Huang-Rhys parameter (S), the functional form of its size dependence well follows that of the LO mode. The coupling can alternatively be recast into energy units (reorganization energy, λ), which follow a slightly different functional form for the LA mode [Fig. 7(c)]. The differences between the size dependences of S and λ for the LA mode merely reflect the size dependence of the LA-mode frequency.

The weak size dependence of the LO coupling strength is qualitatively consistent with recent photon echo experiments. These data do not follow the absolute value or size dependence from Raman experiments since the experiments do not probe the same states (see below). As such one should not compare the LO coupling using femtosecond and CW spectroscopies. There has been no experiment, femtosecond or CW, which measured the size dependence of the coupling to the LA mode.

In terms of comparison to theory, the LO modes were predicted to have either extremely large or vanishingly small couplings. Similarly the size dependence could follow any functional form. While the theoretical underpinnings of the coupling generally agree with each other, the subtleties in electronic structure can yield dramatic differences in the computed couplings. For this reason, experimental determination of the exciton-phonon couplings offers value as a test of the extent to which the electronic structure of quantum dots is well understood.

D. Comparison of time-domain and frequency-domain measurements of coupling strengths

We use the time dependent theory of molecular spectroscopy of Heller *et al.*[73] (see also Refs. 74–76) to simulate the resonance Raman and PL experiments within the Franck-Condon approximation. The methods described below are commonly used in the analysis of molecular spectra and were used in early resonance Raman analysis of CdSe quantum dots by Shiang *et al.*[11] In brief, the calculations below allow one to obtain the phonon progressions in PL experiments and overtone/fundamental ratios in Raman experiments based upon variable parameters such as the exciton-phonon coupling.

In this formulation the polarizability is written in the time domain as a half-Fourier transform of the appropriate autocorrelation function,

$$(\alpha_{fi}(\omega,Q_k))_{\rho\sigma}=\frac{i}{\hbar}\int_0^\infty \langle f|i(t)\rangle e^{i/\hbar(\varepsilon_L-\varepsilon_i+i\Gamma)t}dt, \tag{13}$$

where

$$\langle f|i(t)\rangle=\langle f|\mu_{\rho,iv}e^{-i/\hbar\hat{H}_V t}\mu_{\sigma,vi}|i\rangle. \tag{14}$$

In this equation, the initial vibrational state is promoted to the intermediate excited state, V, at which point it is propagated by the Hamiltonian appropriate for V. The state evolves in time and relaxes to the final state, f. The states $|i\rangle$ and $|f\rangle$ are the full Born-Oppenheimer eigenstates of the ground-state vibronic Hamiltonian. This equation may be simplified by invoking the Born-Oppenheimer approximation and the Condon approximation to produce

$$(\alpha_{fi}(\omega,Q_k))_{\rho\sigma}=\frac{i}{\hbar}(\mu_\rho^0)_{IV}(\mu_\sigma^0)_{VI}\int_0^\infty \langle\phi_f|\phi_i(t)\rangle \times e^{i/\hbar(\varepsilon_L-\varepsilon_i+i\Gamma)t}dt, \tag{15}$$

while for absorption the intensity goes as

$$I(\omega)=\frac{4\pi e^2(\mu^0)_{IV}\omega_L}{6\hbar^2 cn}\int_{-\infty}^\infty \langle\phi_i|\phi_i(t)\rangle e^{i/\hbar(\varepsilon_L-\varepsilon_i)t-\Gamma/\hbar|t|}dt. \tag{16}$$

The PL spectra are computed via complex conjugates in the absorption autocorrelator. In this notation the Born-Oppenheimer approximation is expressed as $|i\rangle=|I\rangle|\phi_i\rangle$ and $|f\rangle=|I\rangle|\phi_f\rangle$. In these equations I and V refer to the ground and excited pure electronic states. The ϕ's refer to the vibrational wave packets which are eigenstates of the ground-state vibronic Hamiltonian. ε_L is the incident photon energy, ε_i is the zero-point vibrational energy, and n is the index of refraction. The prefactors such as $(\mu_\rho^0)_{IV}$ refer to the pure electronic transition moment integrals between states I and V, evaluated at the equilibrium molecular geometry along some Cartesian coordinate ρ.

The autocorrelation function describes the promotion of the initial vibrational state wave packet onto the excited-state potential-energy surface (PES). This wave packet evolves in time due to a displaced, distorted excited-state PES. Its autocorrelation with respect to the chosen final-state wave packet may be computed. Upon invoking the assumptions of two identical harmonic potential-energy surfaces, where the minimum of the excited-state PES is shifted along each normal coordinate by a value Δ_k (in dimensionless normal coordinates) for the kth mode, Heller *et al.*[73] arrived at the following equation for the autocorrelator:

$$\langle\phi_f|\phi_i(t)\rangle=\prod_k\left\{\exp\left[-\frac{\Delta_k^2}{2}[1-\exp(i\omega_k t)]-\frac{i\omega_k t}{2}\right]\times[1-\exp(-i\omega_k t)]^{n_k}(-1)^{n_k}\Delta^{n_k}(2^{n_k}n_k!)^{-1/2}\right\}. \tag{17}$$

The value of n_k refers to the quanta excited in each mode k. The frequencies ω_k and ω_0 refer to the vibrational mode and the 0-0 energy, respectively.

This approach allows one to compute the Raman and PL spectra based upon knowledge of the coupling strengths and electronic dephasing rates. Using the LO and LA couplings from these experiments and the room-temperature homogeneous linewidth ($\Gamma=100$ meV) from recent echo peak shift experiments,[8,9] we compute the resonance Raman spectrum based upon these parameters in Fig. 8(a). This value of Γ is larger than that used by Shiang *et al.*,[11] yielding a larger $\Delta\sim 3$. The computed spectra show that the LA mode is weak relative the LO mode, and the overtone of the LO mode is also weak. Similarly, there are no combinations of LA+LO observed.

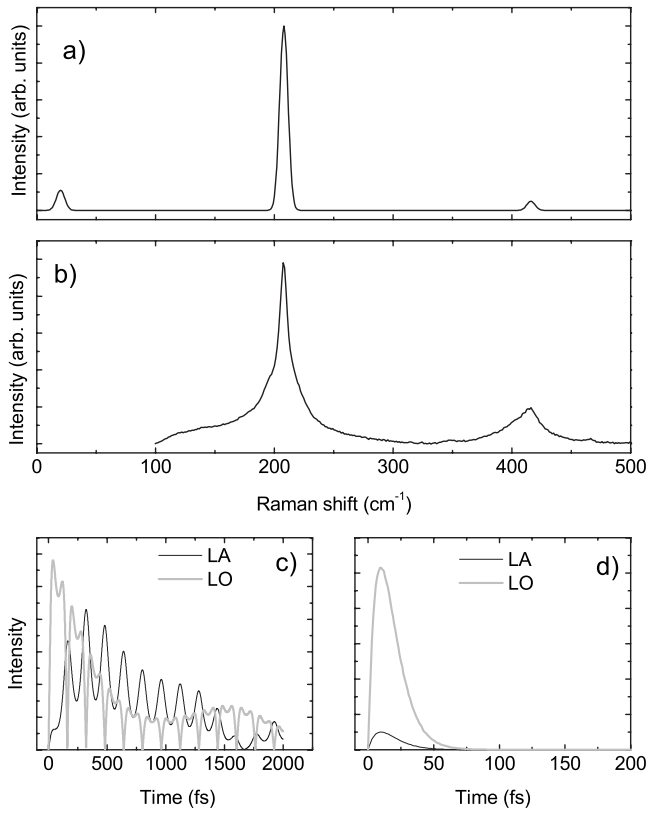

FIG. 8. Exciton-phonon coupling as probed by resonance Raman spectroscopy. (a) A resonance Raman spectrum simulated from the coupling parameters obtained from the femtosecond experiments. (b) The experimental spectrum of CdSe quantum dots in toluene with their native ligands. (c) Raman correlation functions for the LA and LO modes with a homogeneous linewidth of 5 cm^{-1} and the equal coupling. The half-Fourier transform of this correlation function gives the Raman intensity. (d) The same correlation functions with a linewidth of 500 cm^{-1}, corresponding to the room-temperature homogeneous linewidths obtained from photon echo experiments (Ref. 8). The LA mode has an attenuated correlation function by the fast electronic dephasing time.

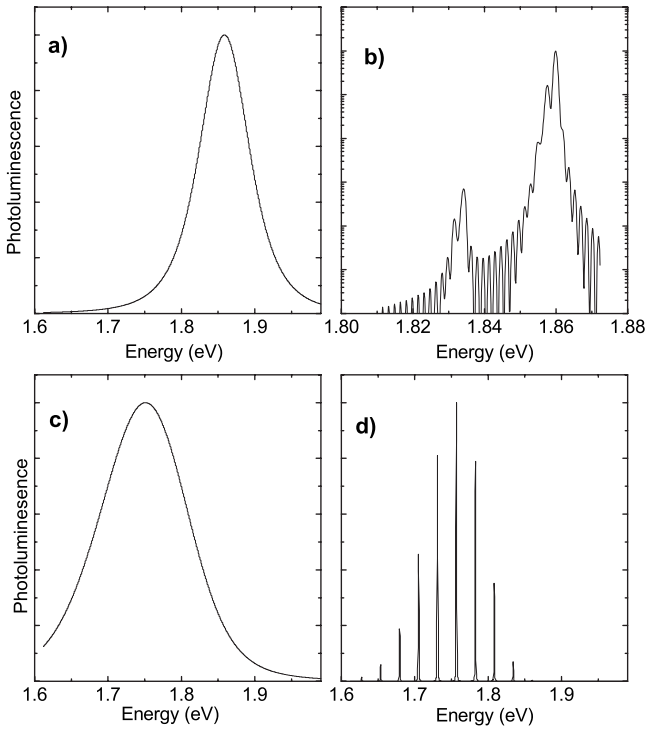

FIG. 9. A comparison of the photoluminescence spectra simulated from the intrinsic (time-domain) and extrinsic (frequency-domain) measures of the exciton-phonon coupling strength. (a) The simulated absorption spectrum based upon couplings from the femtosecond data. This spectrum corresponds to a purely homogeneously broadened spectrum—a single dot at room temperature. (b) The same as (a) but with 0.8 meV linewidth in order to show the LA and LO modes. Note that the spectrum is shown on a logarithmic scale with a smaller energy scale to illustrate the phonon progressions. (c) The same as (a), using the couplings from the resonance Raman experiments. (d) The same as (b), using the couplings from the resonance Raman experiments.

These calculated spectra are quite different from the experimental Raman spectra [Fig. 8(b)]. These experimental resonance Raman spectra are entirely consistent with prior works in terms of the overtone/fundamental ratios.[10–12] The discrepancy between the time-domain and the frequency-domain results may be fundamental to the states being probed in each experiment, further discussed below.

The difference between the LA amplitude and the LO amplitude in the calculated spectra are easy to understand within the time dependent picture of Heller *et al.*[73] The Raman amplitude is based upon not only the coupling strength but also the electronic dephasing time *relative* to the vibrational period. In particular, the Raman autocorrelator begins at zero and grows to a maximum and oscillates on the time scale of a given mode. In this case, the LA mode may have stronger intrinsic coupling. However, its autocorrelator gets damped before it develops much amplitude. Figures 8(c) and 8(d) show the Raman correlation functions with and without damping. Both the LO and LA modes were given the same coupling to illustrate the effect of dephasing. The Fourier transform of this amplitude reflects the Raman intensity. Thus the time dependent picture can explain why the LA modes have smaller Raman amplitude despite their larger couplings. The small LO overtone and small combination tones are due to the small couplings.

The photoluminescence spectra can be computed once the couplings are known. Figure 9 compares the simulated PL spectra based upon the time-domain (pump/probe) and frequency-domain (resonance Raman) based couplings. The PL spectra here correspond to a single particle; i.e., no inhomogeneous broadening was included. The spectrum in Fig. 9(b) shows LA sidebands that are similar in amplitude to the recent single dot PL experiments.[18,49]

In contrast, the PL spectra computed based upon the Raman obtained couplings show extremely large progressions [Fig. 9(d)], corresponding to $S=4.5$. However, this value of S may be too large by omission of Jahn-Teller contributions to the scattering cross section.[77] Essentially, the observed Raman intensities may have contributions via vibronic mixing of other electronic states. This mixing reduces the total adiabatic coupling required to simulate the experimental data.[77] The Raman based couplings should be viewed as an upper limit of the CW based coupling.

Experimental single particle PL spectra can show LO progressions between those shown in Figs. 9(b) and 9(d).[21] These experimental spectra can show the LO sideband intensity changing during the course of the experiment, with an extracted coupling strength that fluctuates by ~20 times *for a single dot*.[21] Here, the couplings range from 0.06 to 1.3, with a mean value of 0.48. Interestingly, the *minimal* S_{LO} from these PL experiments is within a factor of 2 of our time-domain measurements. This observation suggests that these CW experiments measure some fluctuating quantity that may not represent the intrinsic states of the quantum dot.[21,51,52]

E. Intrinsic versus extrinsic coupling

The idea of intrinsic and extrinsic exciton-phonon coupling was introduced by Wise[5] and Krauss and Wise.[6] Here, we further explore this idea as the system evolves from the pump prescribed initial excitonic state to some final surface trapped state. The subject of exciton relaxation dynamics has been under intense experimental and theoretical investigation. Our recent work on state-to-state exciton dynamics has shown that it is possible to monitor electron and hole transition rates between *specific* initial and final states.[30,34,35] This approach has yielded a measure of the *state-resolved* transition rates for the excitonic manifold.

Given the initial excitonic state populated by a pump pulse and given knowledge of the relevant states and their transition rates, one can compute the time dependent populations as the system relaxes down the excitonic manifold and ultimately undergoes surface trapping. Based upon the time dependent populations and the state dependent coupling strengths, one can obtain the population averaged effective coupling strength [Fig. 10]. The state-resolved LO couplings are shown in Fig. 10(a) and the time dependent populations are shown in Fig. 10(b). We denote the effective coupling as

$$\langle S(t)\rangle = \sum_i P_i(t) \times S_i. \tag{18}$$

The system starts with weak LO coupling, which subsequently increases on multiple subpicosecond time scales as the hot exciton relaxes to the band-edge exciton. The band-edge exciton eventually gets surface trapped on the 10–100 ps time scale.[29,30,34,35,56,78] The manifold of core states are the intrinsic couplings probed by these femtosecond experiments. In contrast, the CW experiments probe the *time integral* of the effective coupling,

$$S_{\mathrm{CW}} = \int_0^\infty \langle S(t)\rangle dt. \tag{19}$$

The CW coupling is dominated by the surface trapped state. The differences between the femtosecond experiments and the CW experiments are a question of *time scale*. As such, the difference between the intrinsic and extrinsic states and their characteristic parameters is also a question of time scale.

This proposition that the CW experiments measure a time averaged effective coupling is consistent with the Raman and single dot PL results. In the case of Raman, one measures the ensemble averaged time integral of the coupling. This coupling may fluctuate to large values do to charge trapping. The Raman results in Fig. 5 are consistent with this idea, as the passivations which facilitate hole trapping (pyridine) result in larger coupling, whereas the passivations which reduce carrier trapping (ZnS) have smaller couplings than the dots with their standard passivation (HDA+TOPO). Similarly, the fluctuating LO couplings from the single dot PL experiments[21] are consistent with the idea of CW experiments monitoring a time averaged quantity with large contributions from some extrinsic coupling.

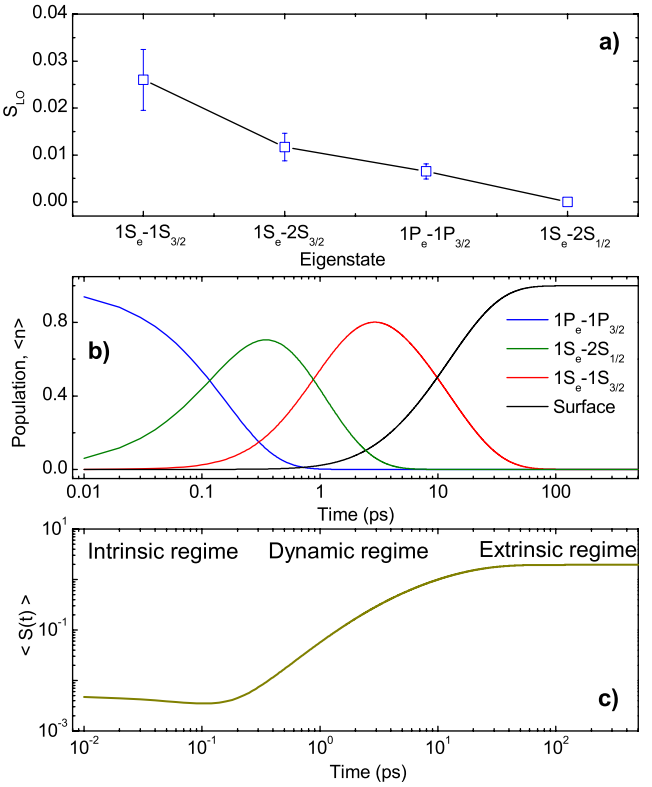

FIG. 10. (Color online) Illustration of dynamic exciton-phonon coupling which addresses the different quantities measured in time-domain and frequency-domain experiments. (a) The coupling to optical phonons as a function of excitonic state. (b) The populations as a function of time. (c) The population averaged coupling $\langle S(t)\rangle$ is time dependent.

As a final point, knowledge of the time evolution of the effective coupling and the physical mechanism of the LO coupling suggests some interesting predictions. The Fröhlich coupling is due to the charge distribution of the exciton. The time evolution of the coupling therefore reflects the time evolution of the charge distribution. The specific time scales of excitonic relaxation suggest that time dependent polarization will be created which should radiate at terahertrz frequencies.

VI. CONCLUSIONS

We report on size and state-resolved exciton-phonon couplings in strongly confined CdSe quantum dots. Femtosec-

ond pump/probe experiments yielded the first simultaneous observation of coherent optical and acoustic phonons in this canonical system for quantum dot studies. Upon excitation directly into the band-edge exciton, both optical and acoustic modes produce nearly equal oscillation amplitudes. Upon excitation into higher-lying states, the optical modes dramatically attenuate in amplitude, reflecting the excitonic state dependence of the Fröhlich interaction. In contrast, the acoustic modes are only weakly attenuated. The state dependent experiments suggest an origin for the discrepancies between time-domain experiments for observing coherent phonons in quantum dots, as well as indicate the value of keeping the state constant for size dependent studies. The size dependence of the coupling of the modes to the band-edge exciton is reported. The size and state dependent couplings are compared to theory and related experiments. These time-domain experiments yield couplings that are completely at odds with frequency-domain experiments, which, in this case, are resonance Raman. The discrepancy is addressed in terms of state-resolved exciton-phonon couplings. Time-domain experiments measure the intrinsic coupling strengths, whereas CW experiments measure the time integrated couplings, which effectively yields the extrinsic coupling strengths. We find that the distinction between intrinsic (quantized core) states and extrinsic (trapped) states is a question of time scale.

ACKNOWLEDGMENTS

Financial support from the CFI, NSERC, FQRNT, and McGill University is acknowledged. The authors thank the McGill University Center for Self-Assembled Chemical Structures for use of their facilities. S.L.S. acknowledges support from McGill University. E.A.D. acknowledges support from NSERC. The authors thank Alexander Efros for helpful comments and Jonathan Mooney for assistance with some experiments.

*Author to whom correspondence should be addressed; pat.kambhampati@mcgill.ca

[1] A. P. Alivisatos, J. Phys. Chem. **100**, 13226 (1996).
[2] V. I. Klimov, Annu. Rev. Phys. Chem. **58**, 635 (2007).
[3] A. L. Efros and M. Rosen, Annu. Rev. Mater. Sci. **30**, 475 (2000).
[4] A. J. Nozik, Annu. Rev. Phys. Chem. **52**, 193 (2001).
[5] F. W. Wise, Acc. Chem. Res. **33**, 773 (2000).
[6] T. D. Krauss and F. W. Wise, Phys. Rev. Lett. **79**, 5102 (1997).
[7] T. D. Krauss and F. W. Wise, Phys. Rev. B **55**, 9860 (1997).
[8] M. R. Salvador, M. W. Graham, and G. D. Scholes, J. Chem. Phys. **125**, 184709 (2006).
[9] M. R. Salvador, M. A. Hines, and G. D. Scholes, J. Chem. Phys. **118**, 9380 (2003).
[10] D. M. Mittleman, R. W. Schoenlein, J. J. Shiang, V. L. Colvin, A. P. Alivisatos, and C. V. Shank, Phys. Rev. B **49**, 14435 (1994).
[11] J. J. Shiang, S. H. Risbud, and A. P. Alivisatos, J. Chem. Phys. **98**, 8432 (1993).
[12] A. P. Alivisatos, T. D. Harris, P. J. Carroll, M. L. Steigerwald, and L. E. Brus, J. Chem. Phys. **90**, 3463 (1989).
[13] G. Cerullo, S. De Silvestri, and U. Banin, Phys. Rev. B **60**, 1928 (1999).
[14] D. H. Son, J. S. Wittenberg, U. Banin, and A. P. Alivisatos, J. Phys. Chem. B **110**, 19884 (2006).
[15] E. R. Thoen, G. Steinmeyer, P. Langlois, E. P. Ippen, G. E. Tudury, C. H. Brito Cruz, L. C. Barbosa, and C. L. Cesar, Appl. Phys. Lett. **73**, 2149 (1998).
[16] M. J. Seong, O. I. Micic, A. J. Nozik, A. Mascarenhas, and H. M. Cheong, Appl. Phys. Lett. **82**, 185 (2003).
[17] P. Palinginis, S. Tavenner, M. Lonergan, and H. Wang, Phys. Rev. B **67**, 201307(R) (2003).
[18] G. Chilla, T. Kipp, T. Menke, D. Heitmann, M. Nikolic, A. Fromsdorf, A. Kornowski, S. Forster, and H. Weller, Phys. Rev. Lett. **100**, 057403 (2008).
[19] T. J. Liptay, L. F. Marshall, P. S. Rao, R. J. Ram, and M. G. Bawendi, Phys. Rev. B **76**, 155314 (2007).
[20] R. Heitz, I. Mukhametzhanov, O. Stier, A. Madhukar, and D. Bimberg, Phys. Rev. Lett. **83**, 4654 (1999).
[21] S. A. Empedocles, D. J. Norris, and M. G. Bawendi, Phys. Rev. Lett. **77**, 3873 (1996).
[22] A. L. Efros, A. I. Ekimov, F. Kozlowski, V. Petrova-Koch, H. Schmidbaur, and S. Shumilov, Solid State Commun. **78**, 853 (1991).
[23] M. C. Klein, F. Hache, D. Ricard, and C. Flytzanis, Phys. Rev. B **42**, 11123 (1990).
[24] S. Nomura and T. Kobayashi, Phys. Rev. B **45**, 1305 (1992).
[25] S. Schmitt-Rink, D. A. B. Miller, and D. S. Chemla, Phys. Rev. B **35**, 8113 (1987).
[26] T. Takagahara, J. Lumin. **70**, 129 (1996).
[27] T. Takagahara, Phys. Rev. Lett. **71**, 3577 (1993).
[28] D. V. Melnikov and W. B. Fowler, Phys. Rev. B **64**, 245320 (2001).
[29] V. I. Klimov, J. Phys. Chem. B **104**, 6112 (2000).
[30] R. R. Cooney, S. L. Sewall, E. A. Dias, D. M. Sagar, K. E. H. Anderson, and P. Kambhampati, Phys. Rev. B **75**, 245311 (2007).
[31] U. Bockelmann and G. Bastard, Phys. Rev. B **42**, 8947 (1990).
[32] H. Benisty, C. M. Sotomayor-Torres, and C. Weisbuch, Phys. Rev. B **44**, 10945 (1991).
[33] S. S. Prabhu, A. S. Vengurlekar, S. K. Roy, and J. Shah, Phys. Rev. B **51**, 14233 (1995).
[34] R. R. Cooney, S. L. Sewall, K. E. H. Anderson, E. A. Dias, and P. Kambhampati, Phys. Rev. Lett. **98**, 177403 (2007).
[35] S. L. Sewall, R. R. Cooney, K. E. H. Anderson, E. A. Dias, and P. Kambhampati, Phys. Rev. B **74**, 235328 (2006).
[36] P. Guyot-Sionnest, B. Wehrenberg, and D. Yu, J. Chem. Phys. **123**, 074709 (2005).
[37] A. L. Efros, V. A. Kharchenko, and M. Rosen, Solid State Commun. **93**, 281 (1995).
[38] L.-W. Wang, M. Califano, A. Zunger, and A. Franceschetti, Phys. Rev. Lett. **91**, 056404 (2003).
[39] M. Nirmal and L. Brus, Acc. Chem. Res. **32**, 407 (1999).
[40] D. J. Norris, A. L. Efros, M. Rosen, and M. G. Bawendi, Phys.

Rev. B **53**, 16347 (1996).
[41] M. Nirmal, D. J. Norris, M. Kuno, M. G. Bawendi, A. L. Efros, and M. Rosen, Phys. Rev. Lett. **75**, 3728 (1995).
[42] D. J. Norris and M. G. Bawendi, Phys. Rev. B **53**, 16338 (1996).
[43] A. I. Ekimov, F. Hache, M. C. Schanne-Klein, D. Ricard, C. Flytzanis, I. A. Kudryavtsev, T. V. Yazeva, A. V. Rodina, and A. L. Efros, J. Opt. Soc. Am. B **10**, 100 (1993).
[44] A. L. Efros and M. Rosen, Appl. Phys. Lett. **73**, 1155 (1998).
[45] L.-W. Wang and A. Zunger, J. Phys. Chem. B **102**, 6449 (1998).
[46] H. Fu, L.-W. Wang, and A. Zunger, Appl. Phys. Lett. **71**, 3433 (1997).
[47] H. Fu, L.-W. Wang, and A. Zunger, Appl. Phys. Lett. **73**, 1157 (1998).
[48] H. Fu, L.-W. Wang, and A. Zunger, Phys. Rev. B **57**, 9971 (1998).
[49] M. J. Fernee, B. N. Littleton, S. Cooper, H. Rubinsztein-Dunlop, D. E. Gomez, and P. Mulvaney, J. Phys. Chem. C **112**, 1878 (2008).
[50] M. Nirmal, C. B. Murray, and M. G. Bawendi, Phys. Rev. B **50**, 2293 (1994).
[51] S. Empedocles and M. Bawendi, Acc. Chem. Res. **32**, 389 (1999).
[52] S. A. Empedocles and M. G. Bawendi, Science **278**, 2114 (1997).
[53] A. L. Efros (private communication).
[54] W. W. Yu, L. Qu, W. Guo, and X. Peng, Chem. Mater. **15**, 2854 (2003).
[55] K. E. H. Anderson, S. L. Sewall, R. R. Cooney, and P. Kambhampati, Rev. Sci. Instrum. **78**, 073101 (2007).
[56] V. I. Klimov, D. W. McBranch, C. A. Leatherdale, and M. G. Bawendi, Phys. Rev. B **60**, 13740 (1999).
[57] W. T. Pollard, S. L. Dexheimer, Q. Wang, L. A. Peteanu, C. V. Shank, and R. A. Mathies, J. Phys. Chem. **96**, 6147 (1992).
[58] C. J. Bardeen, Q. Wang, and C. V. Shank, J. Phys. Chem. A **102**, 2759 (1998).
[59] P. Kambhampati, D.-H. Son, T. W. Kee, and P. F. Barbara, J. Phys. Chem. A **104**, 10637 (2000).
[60] C. Silva, P. K. Walhout, K. Yokoyama, and P. F. Barbara, Phys. Rev. Lett. **80**, 1086 (1998).
[61] A. P. Alivisatos, T. D. Harris, L. E. Brus, and A. Jayaraman, J. Chem. Phys. **89**, 5979 (1988).
[62] U. Woggon, H. Giessen, F. Gindele, O. Wind, B. Fluegel, and N. Peyghambarian, Phys. Rev. B **54**, 17681 (1996).
[63] Y. Z. Hu, S. W. Koch, M. Lindberg, N. Peyghambarian, E. L. Pollock, and F. F. Abraham, Phys. Rev. Lett. **64**, 1805 (1990).
[64] K. I. Kang, A. D. Kepner, S. V. Gaponenko, S. W. Koch, Y. Z. Hu, and N. Peyghambarian, Phys. Rev. B **48**, 15449 (1993).
[65] S. L. Sewall, R. R. Cooney, D. M. Sagar, and P. Kambhampati (unpublished).
[66] H. J. Zeiger, J. Vidal, T. K. Cheng, E. P. Ippen, G. Dresselhaus, and M. S. Dresselhaus, Phys. Rev. B **45**, 768 (1992).
[67] A. Gambetta, C. Manzoni, E. Menna, M. Meneghetti, G. Cerullo, G. Lanzani, S. Tretiak, A. Piryatinski, A. Saxena, R. L. Martin, and A. R. Bishop, Nat. Phys. **2**, 515 (2006).
[68] D. H. Son, P. Kambhampati, T. W. Kee, and P. F. Barbara, J. Phys. Chem. A **106**, 4591 (2002).
[69] T.-Y. Chen, C.-H. Hsia, H. S. Son, and D. H. Son, J. Am. Chem. Soc. **129**, 10829 (2007).
[70] V. I. Klimov, *Semiconductor and Metal Nanocrystals: Synthesis and Electronic and Optical Properties* (Dekker, New York, 2004).
[71] D. M. Sagar, S. L. Sewall, R. R. Cooney, E. A. Dias, and P. Kambhampati (unpublished).
[72] T. D. Krauss, F. W. Wise, and D. B. Tanner, Phys. Rev. Lett. **76**, 1376 (1996).
[73] E. J. Heller, R. L. Sundberg, and D. Tannor, J. Phys. Chem. **86**, 1822 (1982).
[74] A. B. Myers and R. A. Mathies, in *Biological Applications of Raman Spectroscopy: Resonance Raman Spectra of Polyenes and Aromatics*, edited by T. G. Spiro (Wiley, New York, 1987), Vol. 2, p. 1.
[75] A. B. Myers, Chem. Rev. (Washington, D.C.) **96**, 911 (1996).
[76] A. B. Myers, Chem. Phys. **180**, 215 (1994).
[77] E. P. Pokatilov, S. N. Klimin, V. M. Fomin, J. T. Devreese, and F. W. Wise, Phys. Rev. B **65**, 075316 (2002).
[78] S. L. Sewall, R. R. Cooney, K. E. H. Anderson, E. A. Dias, D. M. Sagar, and P. Kambhampati (unpublished).